THE JOURNAL OF BIOLOGICAL CHEMISTRY
Vol. 277, No. 6, Issue of February 8, pp. 4558–4564, 2002

Printed in U.S.A.

A Helical Region in the C Terminus of Small-conductance Ca^{2+}-activated K^+ Channels Controls Assembly with Apo-calmodulin*

Received for publication, September 25, 2001, and in revised form, November 21, 2001
Published, JBC Papers in Press, November 26, 2001, DOI 10.1074/jbc.M109240200

Ralph Wissmann‡, Wolfgang Bildl‡, Heinz Neumann‡, Andre F. Rivard§, Nikolaj Klöcker‡**, Dietmar Weitz¶, Uwe Schulte‡**, John P. Adelman§, Detlef Bentrop‡**, and Bernd Fakler‡‖**

From the ‡Department of Physiology II, University of Tübingen, Ob dem Himmelreich 7, 72074 Tübingen, Germany, the §Vollum Institute, Oregon Health Science University, Portland, Oregon 97201, and the ¶Institut für Biologische Informationsverarbeitung, Forschungszentrum Jülich, 52452 Jülich, Germany

Small conductance Ca^{2+}-activated potassium (SK) channels underlie the afterhyperpolarization that follows the action potential in many types of central neurons. SK channels are voltage-independent and gated solely by intracellular Ca^{2+} in the submicromolar range. This high affinity for Ca^{2+} results from Ca^{2+}-independent association of the SK α-subunit with calmodulin (CaM), a property unique among the large family of potassium channels. Here we report the solution structure of the calmodulin binding domain (CaMBD, residues 396–487 in rat SK2) of SK channels using NMR spectroscopy. The CaMBD exhibits a helical region between residues 423–437, whereas the rest of the molecule lacks stable overall folding. Disruption of the helical domain abolishes constitutive association of CaMBD with Ca^{2+}-free CaM, and results in SK channels that are no longer gated by Ca^{2+}. The results show that the Ca^{2+}-independent CaM-CaMBD interaction, which is crucial for channel function, is at least in part determined by a region different in sequence and structure from other CaM-interacting proteins.

Small conductance Ca^{2+}-activated potassium (SK)[1] channels are responsible for the prolonged afterhyperpolarization that follows the action potential in many central neurons and is a major determinant of excitability and firing pattern (1–4). SK channels are voltage-independent and activated by an increase in intracellular Ca^{2+} concentration ($[Ca^{2+}]_i$) such as occurs during an action potential (5, 6).

Three highly homologous mammalian SK channels (SK1, SK2, and SK3) have been cloned (7), as well as a related channel with an intermediate conductance (IK1) (8, 9). SK subunits share the prototypic membrane topology of voltage-gated K^+ (Kv) channels with six transmembrane domains flanked by cytoplasmic N and C termini (Fig. 1), although their primary sequences do not contain any significant homology outside the P-loop. As for their native counterparts, cloned SK channels are solely gated by $[Ca^{2+}]_i$ in the submicromolar range, independent of the transmembrane voltage (7, 10–12).

Analysis of Ca^{2+}-gating showed that the high affinity of SK channels for Ca^{2+} results from a property, unique among the large family of K^+ channels: the SK α-subunits associate with the Ca^{2+}-binding protein calmodulin (CaM) (12). This association is constitutive, *i.e.* it occurs in the absence of Ca^{2+}. In this context, activation of SK channels results from Ca^{2+} binding to CaM, which induces conformational changes in both molecules that finally lead to opening of the channel pore (11, 12).

Accordingly, channel-gating requires both, Ca^{2+}-independent and Ca^{2+}-dependent interaction between SKα and CaM. For either type of interaction, functional analysis identified distinct domains on the CaM molecule. Ca^{2+} binding occurs only in the N-terminal EF-hands of CaM, while the C-terminal lobe mediates Ca^{2+}-independent interactions with the SK α-subunits (11). Both types of interactions with CaM require a domain of about 90 amino acids in the proximal C terminus of the channel subunit, the calmodulin binding domain (CaMBD, Fig. 1). As long as the CaMBD is present at the C terminus of the SK α-subunit, channels exhibit regular Ca^{2+}-gating; deletions of more than 10 residues (marked by an asterisk in Fig. 1) resulted in channels that were no longer gated by intracellular Ca^{2+} (12).

As illustrated in Fig. 1, the CaMBD is highly conserved among the SK subunits, but shows no clear homology with any other known protein (7). Different from other CaM-binding proteins, the CaMBD sequence does not provide a canonical motif for either Ca^{2+}-free or Ca^{2+}-dependent interactions with CaM (13–16).

Recently we have reported the crystal structure of the Ca^{2+}-loaded complex between CaMBD and CaM (17). In the presence of Ca^{2+} this complex presents as a dimer formed by two CaMBDs and two CaMs with each CaMBD molecule interacting with two CaM molecules. In contrast to this "gated complex" the Ca^{2+}-free CaMBD·CaM complex is a monomer as shown by sedimentation analysis (see supplemental information in Ref. 17). For this monomer, however, as well as for the uncomplexed CaMBD no direct structural information is available. In this report we present the solution structure of the SK2 CaMBD and show that a distinct region is important for the unique Ca^{2+}-free interaction with CaM.

* This work was supported by the Deutsche Forschungsgemeinschaft Grant Fa332/3-1), the Federal Ministry of Education, Science, Research, and Technology Grant Fö.01KS9602, and the Interdisciplinary Center of Clinical Research (IZKF) Tübingen, Germany (Project IA4) (to B. F.). The costs of publication of this article were defrayed in part by the payment of page charges. This article must therefore be hereby marked "*advertisement*" in accordance with 18 U.S.C. Section 1734 solely to indicate this fact.

The atomic coordinates (code 1KKD) have been deposited in the Protein Data Bank, Research Callaboratory for Structural Bioinformatics, Rutgers University, New Brunswick, NJ (http://www.rcsb.org/).

‖ To whom correspondence should be addressed: Dept. of Physiology II, Ob dem Himmelreich 7, 72074 Tübingen, Germany. Tel.: 49-7071-297-7173; Fax: 49-7071-87815; E-mail: bernd.fakler@uni-tuebingen.de.

** Current address: Dept. of Physiology II, University of Freiburg, Hermann-Herder-Str. 7, 79104 Freiburg, Germany.

[1] The abbreviations used are: SK, small conductance Ca^{2+}-activated K^+ channel; CaM, calmodulin; CaMBD, calmodulin binding domain of SK channels; HSQC, heteronuclear single-quantum coherence; NOESY, nuclear Overhauser effect spectroscopy; NOE, nuclear Overhauser enhancement; HNHA, amide proton to nitrogen to α proton correlation; MES, 4-morpholineethanesulfonic acid; PBS, phosphate-buffered saline; BAPTA, 1,2-bis(*O*-aminophenoxy)ethane-*N*,*N*,*N*′,*N*′-tetraacetic acid; r.m.s.d, root mean square deviation.

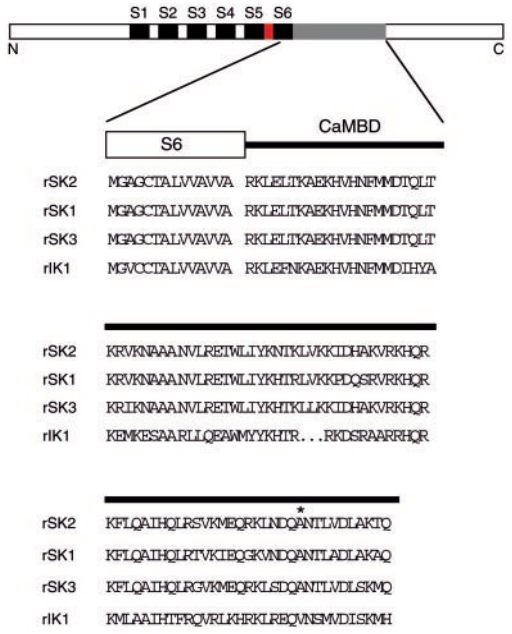

FIG. 1. **CaMBD in SK-type K^+ channels.** Sequence alignment of rat SK channels; the transmembrane topology is given above the sequences (P-loop is *red colored*). The sequences are rSK2 (GenBank™ accession number U69882), rSK1 (GenBank™ accession number U69885), rSK3 (GenBank™ accession number U69884), rIK1 (GenBank™ accession number AF156554); residue numbers of CaMBD are the following: SK2, 396–487; SK1, 363–457; SK3, 545–636, IK1, 285–373. The asterisk denotes the largest C-terminal deletion of SK2 resulting in Ca^{2+}-gated channels (12).

MATERIALS AND METHODS

Sample Preparation—Uniformly ^{15}N-labeled, and ^{13}C,^{15}N-labeled wild type or mutant CaMBD of rSK2 (residues 396–487 (7) N-terminally extended by Met and Gly and C-terminally by Leu, Glu, and six His) were obtained from overexpression in the *Escherichia coli* strain BL21DE3 codonPlus RIL (Stratagene) and purified to homogeneity via Ni-NTA-agarose (Qiagen). Protein samples of CaMBD were dissolved in 250 mM NaCl (90% H_2O/10% D_2O (v/v)) with trace amounts of NaN_3 as a preservative at pH 3.5 or pH 5; sample concentration was between 1.2 and 0.5 mM.

For interaction studies with apoCaM, samples of unlabeled and uniformly ^{13}C,^{15}N-labeled, 60–70% ^2H-enriched CaMBD were prepared. CaM (from rat) in unlabeled, uniformly ^{15}N-labeled, and uniformly ^{13}C,^{15}N-labeled form was obtained from overexpression in the *E. coli* strain BL21(DE3) and purified to homogeneity by phenyl-Sepharose chromatography. Ca^{2+}-free conditions of NMR samples for CaMBD and CaM were obtained by extensive dialysis against a Ca^{2+}-free 250 mM NaCl solution (passage over a freshly regenerated chelex column prior to dialysis). Small amounts of HCl and NaOH were used to adjust the pH value of these solutions to 6.0.

The apo(CaMBD·CaM) complex was reconstituted by adding aliquots of CaMBD to a CaM-containing solution to a molar ratio of 1:1. In a consecutive step, the complex was concentrated to 0.7–2 mM by ultrafiltration in Centricon tubes, and the pH value was readjusted to 6.0. Final samples of the complex were in 250 mM NaCl (90% H_2O/10% D_2O (v/v), pH 5 or 6) with no buffer salts present. Trace amounts of NaN_3 were added as a preservative. 2,2-dimethyl-2-silapentane-5-sulfonate was added and used for chemical shift referencing.

NMR Spectroscopy—The following three-dimensional NMR spectra were recorded at 298 K on a Bruker Avance 600 spectrometer for the sequence-specific assignment of CaMBD: HNCA, CBCA(CO)NH, CBCANH, HNCO, HN(CA)CO, ^{15}N total correlation spectroscopy-HSQC (70 ms isotropic mixing time), and ^{15}N NOESY-HSQC (100 ms mixing time). Distance restraints for structure calculations were obtained from a three-dimensional ^{15}N NOESY-HSQC (recorded on a Bruker Avance 800) and from two-dimensional homonuclear NOESY experiments in H_2O and 99.9% D_2O solution, respectively; a mixing time of 150 ms was used in all these experiments. $^3J_{HN\text{-}H\alpha}$ coupling constants were determined from a three-dimensional HNHA spectrum. The heteronuclear ^1H-^{15}N NOE was measured at 500 and 600 MHz for wild type CaMBD and at 600 MHz for the mutant CaMBD. A three-dimensional ^{15}N NOESY-HSQC spectrum (150 ms mixing time) of the mutant was recorded at 600 MHz and used to obtain the sequence-specific assignment and distance restraints. H/D exchange of CaMBD was performed by solvent exchange using a NAP5 column (Amersham Biosciences, Inc.).

For assignment of CaMBD backbone resonances in the apo(CaMBD·CaM) complex the following three-dimensional spectra were recorded from samples of labeled CaMBD bound to unlabeled apoCaM (pH 5.0, 298 K): HNCO, HNCA, HN(CO)CACB, TROSY-HNCA, and ^{15}N NOESY-HSQC (100 ms mixing time). The backbone resonances of apoCaM in the complex were unambiguously assigned using the following experiments on samples of labeled CaM bound to unlabeled CaMBD (pH 6.0): TROSY-HNCA, TROSY-HN(CO)CA, TROSY-HNCO, HNHA, and ^{15}N NOESY-TROSY (100 ms mixing time). The backbone assignment of uncomplexed apoCaM was based on published data (available at nmr.oci.utoronto.ca/ikura/public_files/shifts/apo_CaM.cs) verified at the solvent conditions of the complex (250 mM NaCl, pH 6.0, 298 K) by a ^{15}N NOESY-HSQC spectrum (100 ms mixing time). All NMR data were processed with XWINNMR and analyzed using the programs AURELIA (Bruker) and XEASY (ETH Zürich) (18).

Structure Calculations and Protein-docking—Structures were calculated with the program DYANA (19), which employs a simulated annealing algorithm in the torsion angle space. Volumes of assigned NOESY cross-peaks were converted into 668 proton-proton upper distance limits by the program CALIBA (20) using five different classes of NOEs (21). The measured 35 values of $^3J_{HN\text{-}H\alpha}$ were used directly as J-coupling restraints. After recalibration of distance restraints in four cycles of preliminary DYANA calculations the final family of structures was generated in a run with 300 random starting structures and 12,000 annealing steps. The 23 best structures had values for the target function <1.25 Å^2, no NOE violations >0.4 Å, and no violations of J-coupling restraints. For the CaMBD mutant, the same restraints as for wild type CaMBD were used, except for the J-coupling restraint of Leu-33, all NOEs involving side chain protons of Val-32 and Leu-33 and NOEs abolished in the three-dimensional ^{15}N NOESY-HSQC of the mutant. Starting from 250 random structures a final family of 15 structures with target function values <1.23 Å^2 and no NOE violations >0.6 Å was obtained. All figures were generated with the program MOLMOL (22) except Fig. 7, which was generated with GRASP (23).

Protein-docking simulations were done with the program GRAMM (v. 1.03) (24) using a standard hydrophobic docking protocol (25). This program employs a geometric recognition algorithm performing an exhaustive six-dimensional search through relative translations and rotations of two molecules in order to provide maximal surface complementarity. For the GRAMM runs, the pseudoatoms originating from DYANA were removed from the CaMBD structure file. The r.m.s.d value of the two best solutions of the docking referred to in "Discussion" was 1.0 Å.

Electrophysiology—SK2 channels were heterologously expressed in *Xenopus* oocytes as described elsewhere (26). Giant patch recordings were made at room temperature (~23 °C) 3–7 days after injection of SK2-specific cRNA. Pipettes used were made from thick-walled borosilicate glass and had resistances of 0.2–0.3 MΩ (tip diameter of about 20 μm) when filled with (in mM) 120 KOH, 10 HEPES and 0.5 $CaCl_2$, pH adjusted to 7.2 with MES. Inside-out patches were superfused with an intracellular solution containing (in mM): 119 KOH, 1 KCl, 10 HEPES, 1 EGTA, pH adjusted to 7.2 with MES; the amount of $CaCl_2$ required to yield a free Ca^{2+} concentration of 10 μM was calculated according to Fabiato (27) and added to the EGTA-solution under pH-meter control; thereafter, pH was readjusted to 7.2 with KOH.

Rapid exchange of Ca^{2+} was achieved using a piezo-driven application system (28); data analysis was performed with IgorPro (WaveMetrics, Lake Oswego, OR) on a Macintosh PowerPC.

Biochemistry and Immunocytochemistry—For probing interaction between CaM and wild type or mutant CaMBD, 250 μg of His-tagged CaMBD protein was incubated at 4 °C with Ni-NTA-agarose beads (Qiagen; 30 μl) in PBS containing 20 mM imidazole. After 2 h the beads were washed three times with PBS in the presence (10 μM) or absence (1 mM BAPTA) of Ca^{2+}. 80 μg of purified rat CaM dissolved in PBS with or without Ca^{2+} was added to the resin and incubated for 2 h at 4 °C. After washing the resin three times with PBS as indicated above, bound protein was eluted with 200 mM imidazole and separated by SDS-PAGE (15% acrylamide).

For immunocytochemistry, oocytes expressing SK2 or SK2(V427G/L428G) channels were defolliculated and fixed in 4% paraformaldehyde in PBS for 2 h at 4 °C. After blocking unspecific antibody binding with normal goat serum, 10 μm of cryostat sections were incubated with a polyclonal anti-rSK2 antiserum raised against a C-terminal epitope of

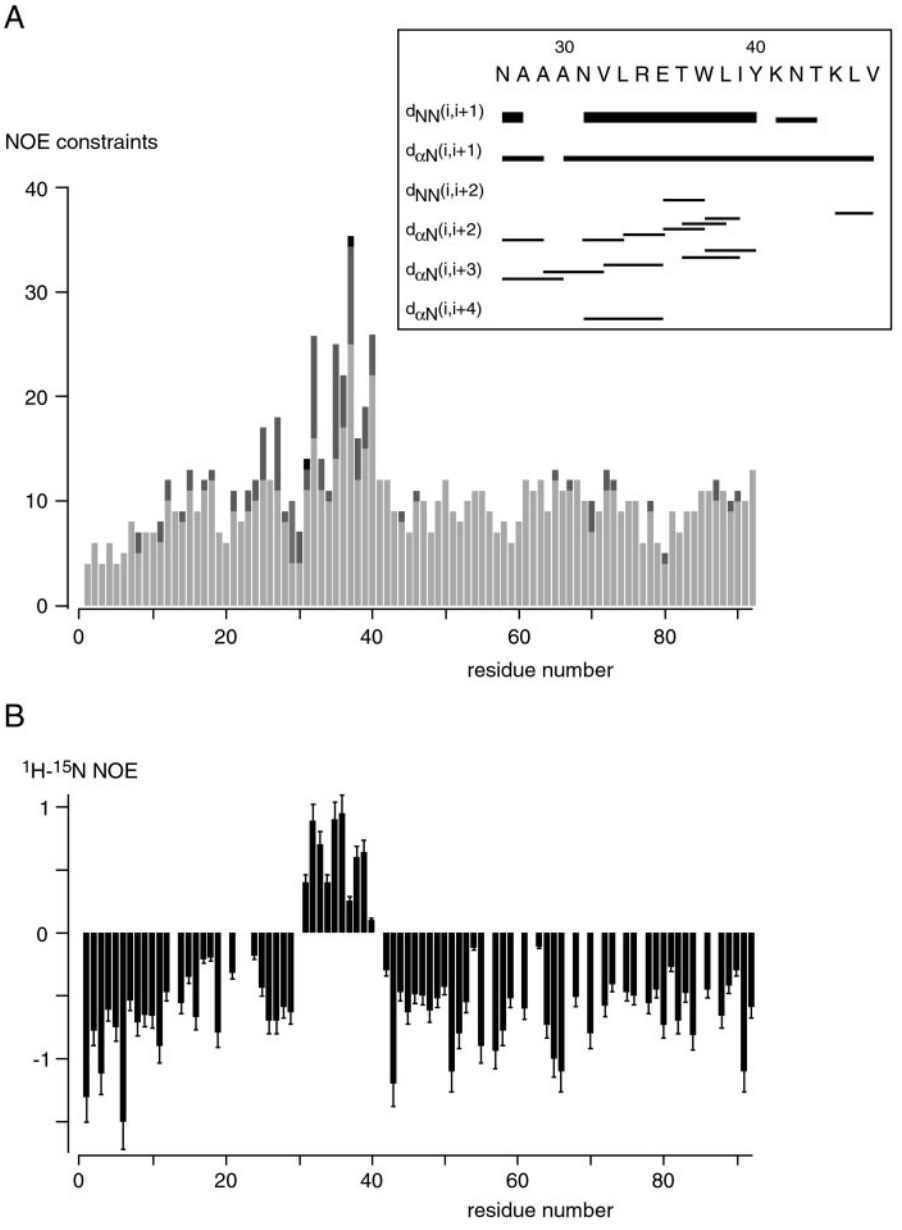

FIG. 2. **NMR data of rSK2 CaMBD.** *A*, bar diagram of NOE constraints by residue. Intraresidual and sequential contacts are drawn in *gray*, medium-range contacts in *dark gray* and long-range contacts in *black*. *Inset*: NOE connectivities between protons of neighboring (d(i, i + 1)) and non-neighboring amino acids in the sequence stretch indicated. Line thickness reflects intensity of NOEs. *B*, ^1H-^{15}N heteronuclear NOE of the CaMBD (measured at 500 MHz); increasing positive values indicate decreasing flexibility of the backbone.

rSK2 (residues 539–558) (29, 30). Immunoreactivity was revealed by cy-3-conjugated secondary anti-rabbit antiserum.

RESULTS

Solution Structure of CaMBD—A histidine-tagged protein containing amino acids 396–487 of the rat SK2 sequence (referred to as residues 1–92 of CaMBD) was purified from bacteria and used for structural evaluation of the CaMBD. The protein formed a stable monomer in a 250-mM NaCl solution as revealed by gel filtration (not shown). A series of multidimensional (two-, three-dimensional) homo- and heteronuclear NMR experiments (see "Materials and Methods") were performed that allowed almost complete assignment of backbone and side chain atoms. The observed NOE connectivities exhibited a distinct distribution along the CaMBD sequence (Fig. 2*A*). For most parts of the molecule an average of ≈10 NOEs was found per residue, while the sequence stretch roughly extending from Ala-28 to Asn-42 exhibited an average of ≈19 NOEs per residue.

Moreover, as shown in Fig. 2*A*, most NOE contacts between non-adjacent amino acids (i, i + x) were found in this part of the CaMBD sequence. Thus, a number of contacts between the α-proton of one amino acid and the amide proton of the second (αN(i, i + 2)) and third amino acid following (αN(i, i + 3)) were observed, a NOE pattern usually found in helical structures. Moreover, most residues throughout this sequence stretch show strong sequential contacts between backbone amide protons (dNN NOEs).

The picture of structurally distinct parts in CaMBD was reinforced by the ^1H-^{15}N heteronuclear NOE, used as a measure for backbone flexibility on the subnanosecond time scale (31). Thus, positive NOE values indicative for increased rigidity were observed for residues between Ala-30 and Tyr-40, while negative values were obtained outside this region (Fig. 2*B*). Together, the NOE pattern and the results from dynamic measurements suggested that CaMBD consists of an ordered most likely helical core region flanked by flexible N and C termini.

All experimentally determined restraints (Tables I and II) were used to calculate the solution structure of the SK2 CaMBD. A family of 22 structures of CaMBD with the lowest target function is shown in Fig. 3*A* for residues 20–50. Thus, CaMBD consists of three parts, non-ordered and flexible N and

TABLE I
Structural statistics of SK2 CaMBD

Structural statistics for the final family of 23 structures. All 92 residues of SK2 CaMBD were included in the analysis. None of the 23 best structures has a target function > 1.25 Å^2, distance restraint violations > 0.4 Å, and violations of J-coupling restraints.

Total number of distance constraints	668
Intraresidual	341
Sequential	272
Medium range ($\|i - j\| \leq 5$)	54
Long range ($\|i - j\| > 5$)	1
$^3J_{HN\text{-}H\alpha}$ coupling constant restraints	35
Distance restraint violations > 0.4 Å (per structure)	0
Coupling constant restraint violations > 0.5 Hz (per structure)	0
Average number of distance restraint violations > 0.2 Å (per structure)	4.0 ± 1.9
Average sum of distance restraint violations (per structure)	4.1 ± 0.6 Å
Average maximum distance restraint violation	0.33 ± 0.05 Å
Average target function	0.96 ± 0.22 Å^2
R.m.s. deviations from the mean structure (superposition of 30–40)	
Backbone heavy atoms	0.71 ± 0.30 Å
All heavy atoms	1.39 ± 0.43 Å

TABLE II
Root mean square deviations from the respective mean structure

Superimposed residues	Backbone heavy atoms	All heavy atoms
	Å	
1–10	2.06 ± 0.57	3.90 ± 0.55
10–20	2.23 ± 0.34	3.86 ± 0.27
20–30	1.88 ± 0.33	3.13 ± 0.52
40–50	2.20 ± 0.61	3.77 ± 0.54
50–60	2.28 ± 0.46	4.21 ± 0.39
60–70	2.41 ± 0.70	3.99 ± 0.61

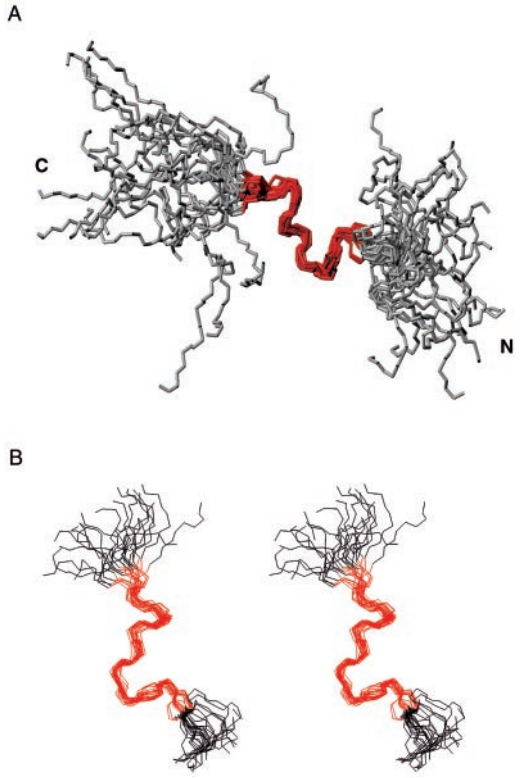

FIG. 3. **Solution structure of the CaMBD.** *A*, backbone traces (N, Cα, C′) of a family of structures (with lowest target function) of the CaMBD between residues 20 and 50. Superposition was calculated for residues 30–40 (highlighted in *red*), N and C termini are indicated. *B*, stereoview of the backbone superposition in *A*, the 22 best structures of the CaMBD between residues 27 and 43 are shown.

C termini flanking an ordered core region that extends between residues 30–40. The core region is well defined with r.m.s.d. values to the mean structure of 0.71 ± 0.30 Å for the backbone atoms and 1.39 ± 0.43 Å for all atoms. It may be best described as series of three helical turns that change sense of rotation in the middle turn (stereoview in Fig. 3*B*). This particular folding was independent of the algorithm used for structure calculations (very similar results were obtained with CNS (32)) and is consistent with the lack of constraints typical for regular helices ($^3J_{HN\text{-}H\alpha}$-couplings < 6 Hz, characteristic chemical shift indices (33)) and the observation of the long-range connectivity between Asn-31 and Trp-37. Alternatively, the experimental NOE data would be consistent with the core region to transiently form a regular three-turn α-helix. The functional significance of this helical region was further investigated by disrupting its folding via site-directed mutagenesis.

Functional Significance of the CaMBD Structure—Two glycine residues were introduced into the isolated CaMBD at positions 32 and 33 (V32G/L33G; Fig. 4, *A* and *B*) as well as into the whole channel molecule (corresponding positions 427 and 428) (34). The mutant CaMBD was examined by NMR and tested for CaM binding, while the mutant channels were tested for Ca^{2+}-gating.

As shown in Fig. 4*A*, these exchanges abolished quite a number of NOE connectivities including all but one of the helix-typical (i, i + 3)-NOEs, as well as the NOEs between Asn-31 and Glu-35 and between Asn-31 and Trp-37. Moreover, the chemical shift of backbone atoms (H_N, H_α, N) between residues 30 and 45 was changed significantly in the mutated CaMBD (Fig. 4*C*), and the ^{1}H-^{15}N heteronuclear NOE indicated a largely increased flexibility of the backbone between residues 30 and 36 (data not shown).

Accordingly, structure calculations (see "Materials and Methods") performed with the restraints derived from the NMR data of the mutant protein yielded significant alterations in the structure of the helical region of CaMBD. As shown in Fig. 4*D*, a family of 15 best structures showed an overall destabilization of this region between residues 30 and 40 with r.m.s.d. values to the mean structure of 2.03 ± 0.58 Å for backbone atoms and 2.69 ± 0.74 Å for all atoms. More detailed analysis of the CaMBD(V32G/L33G) structures showed that there is reasonable convergence only between residues Thr-36 and Lys-41. These residues form an α-helical turn with r.m.s.d. values to the mean structure of 0.59 ± 0.17 Å for backbone atoms and 1.51 ± 0.37 Å for all atoms, very similar to wild type CaMBD. Together, these data indicate that the double glycine exchange leads to structural rearrangements in the CaMBD helical domain that largely destabilize the N-terminal turns between residues Ala-28 and Thr-36, while the most C-terminal turn is roughly conserved.

To examine the functional significance of the helical domain in CaMBD, wild type and mutant CaMBD proteins were probed for their ability to interact with CaM either in the presence (10 μM) or absence (1 mM BAPTA) of Ca^{2+}; in these experiments CaM and CaMBD were used in a molar ratio of about 1:4 (see "Materials and Methods"). As shown in Fig. 5*A*, both CaMBD proteins were able to bind CaM in the presence of Ca^{2+}. Under Ca^{2+}-free conditions, however, CaM-binding was only observed with the wild type CaMBD (Fig. 5*A*). Thus, the mutated CaMBD was no longer able to associate constitutively with CaM. Next the double glycine mutation was introduced at the sites corresponding to Val-32 and Leu-33 in the SK2 sequence (V427G/L428G), and we tested whether the mutated CaMBD altered channel function in the context of the entire

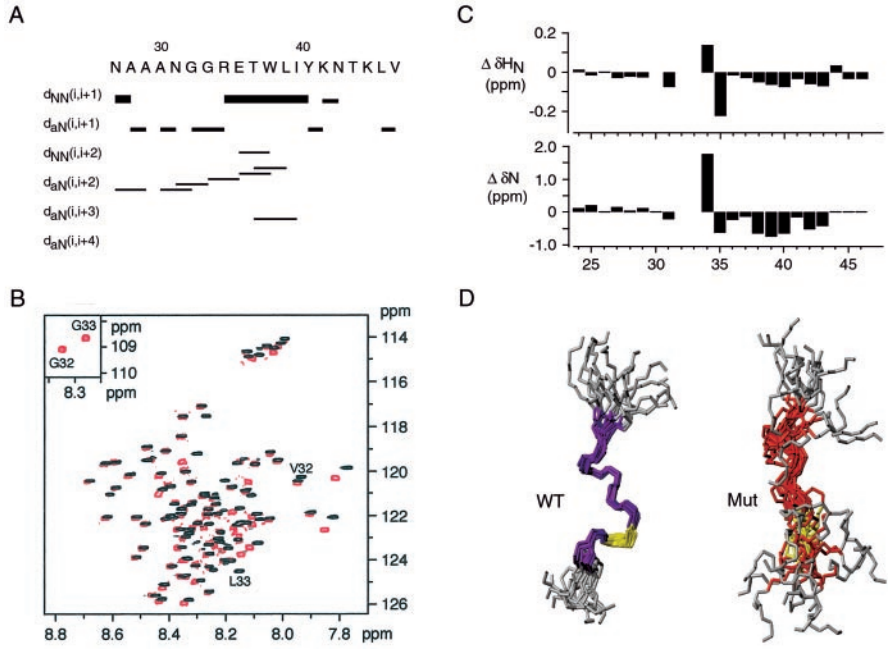

FIG. 4. **Disruption of the CaMBD structure by the V32G/L33G mutation.** *A*, NOE connectivities between protons of neighboring (d(i, i + 1)) and non-neighboring amino acids of the mutant CaMBD (V32G/L33G) in the sequence stretch indicated. *B*, overlay of the ^{1}H-^{15}N HSQC spectra of wild type (*black*) and mutant (*red*) CaMBD. *C*, differences in chemical shift observed for backbone HN groups between wild type and mutant CaMBD on the sequence stretches indicated (residue number on the *x* axis). *D*, backbone superposition of the 15 best structures of wild type and mutant CaMBD between residues 30 and 40. The backbone positions of residues 32 and 33 are highlighted in *yellow*; residues 27–43 are shown.

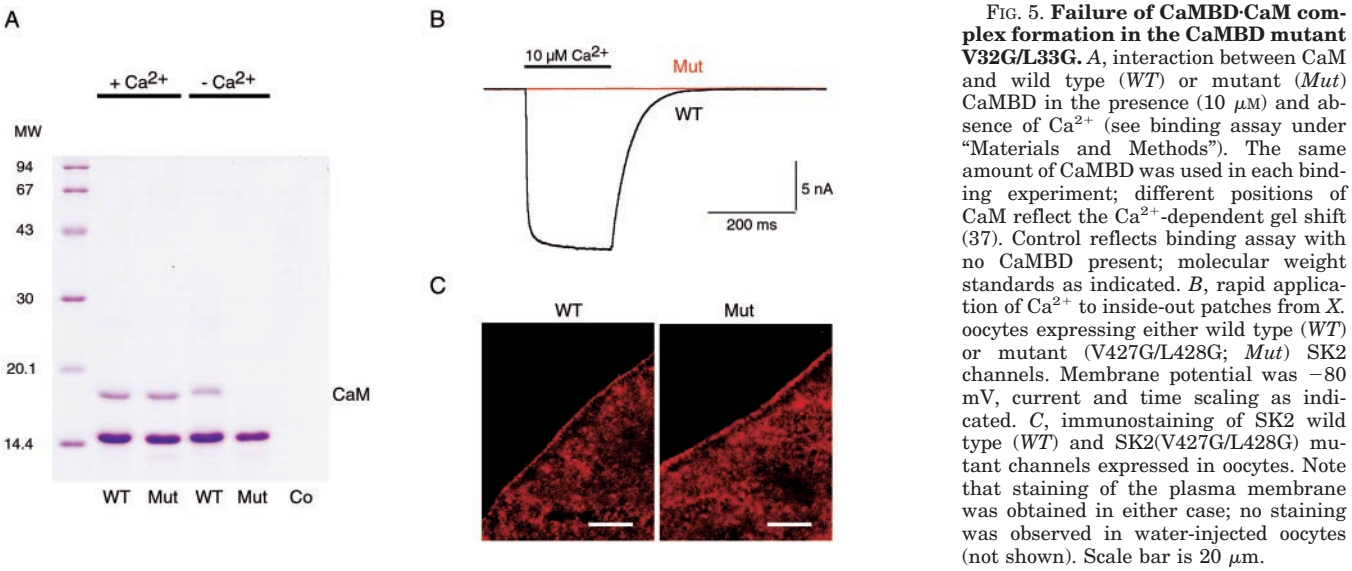

FIG. 5. **Failure of CaMBD·CaM complex formation in the CaMBD mutant V32G/L33G.** *A*, interaction between CaM and wild type (*WT*) or mutant (*Mut*) CaMBD in the presence (10 μM) and absence of Ca^{2+} (see binding assay under "Materials and Methods"). The same amount of CaMBD was used in each binding experiment; different positions of CaM reflect the Ca^{2+}-dependent gel shift (37). Control reflects binding assay with no CaMBD present; molecular weight standards as indicated. *B*, rapid application of Ca^{2+} to inside-out patches from *X. oocytes* expressing either wild type (*WT*) or mutant (V427G/L428G; *Mut*) SK2 channels. Membrane potential was −80 mV, current and time scaling as indicated. *C*, immunostaining of SK2 wild type (*WT*) and SK2(V427G/L428G) mutant channels expressed in oocytes. Note that staining of the plasma membrane was obtained in either case; no staining was observed in water-injected oocytes (not shown). Scale bar is 20 μm.

protein. Fig. 5*B* illustrates representative current recordings obtained in response to fast piezo-driven application of a saturating $[Ca^{2+}]_i$ of 10 μM to inside-out patches excised from *Xenopus* oocytes expressing either wild type or mutant SK2 channels. While large currents were recorded with wild type channels, mutant channels were no longer gated by intracellular Ca^{2+} (n = 52 patches from 12 oocytes). Consistent with the lack of Ca^{2+}-free CaM binding of mutant SK2 subunits, the observed loss of channel function was not due to a loss of subunit assembly or to reduced insertion of SK2 protein into the plasma membrane. Both, wild type and mutant SK2 protein, were equally detected in the plasma membrane of oocytes by immunostaining with an SK2-specific antibody (30) (Fig. 5*C*). Together, these structural and functional data show, that association of SK channels with CaM is at least in part determined by a short helical domain in the proximal C terminus of the SK α-subunit.

Interactions Between CaMBD and ApoCaM—The Ca^{2+}-free association between CaMBD and CaM was examined in NMR experiments on the apo(CaMBD·CaM) complex reconstituted in solution (see "Materials and Methods"). For selective analysis of both components in the complex, either CaMBD or CaM was labeled. Surprisingly, as shown in Fig. 6*A*, the ^{1}H-^{15}N HSQC spectrum of complexed CaMBD only exhibited about a third of the expected 92 amide cross-peaks, which were finally assigned to the very N- and C-terminal residues of the molecule (Arg-1-Met-16 and Gln-81-Gln-92, Fig. 6*B*). The cross-peaks of the remaining amino acids in CaMBD were broadened beyond the detection level. This phenomenon is well known and diagnostic of conformational exchange processes on an intermediate time scale.

Different from CaMBD, all cross-peaks of CaM within the apo(CaMBD·CaM) complex were visible in ^{1}H-^{15}N correlation spectra recorded with the TROSY technique (35). However, while the residues in the N-terminal half of CaM could be assigned by three-dimensional triple resonance experiments, the majority of the C-terminal spin-systems exhibited relaxation rates precluding assignment with conventional and TROSY 3D spectra. As shown by the chemical shift mapping of the backbone amide groups (Fig. 6*C*), the resonances of the residues in the N-terminal half of CaM are hardly perturbed in the apo(CaMBD·CaM) complex indicating that this part of CaM does not participate in the protein-protein association.

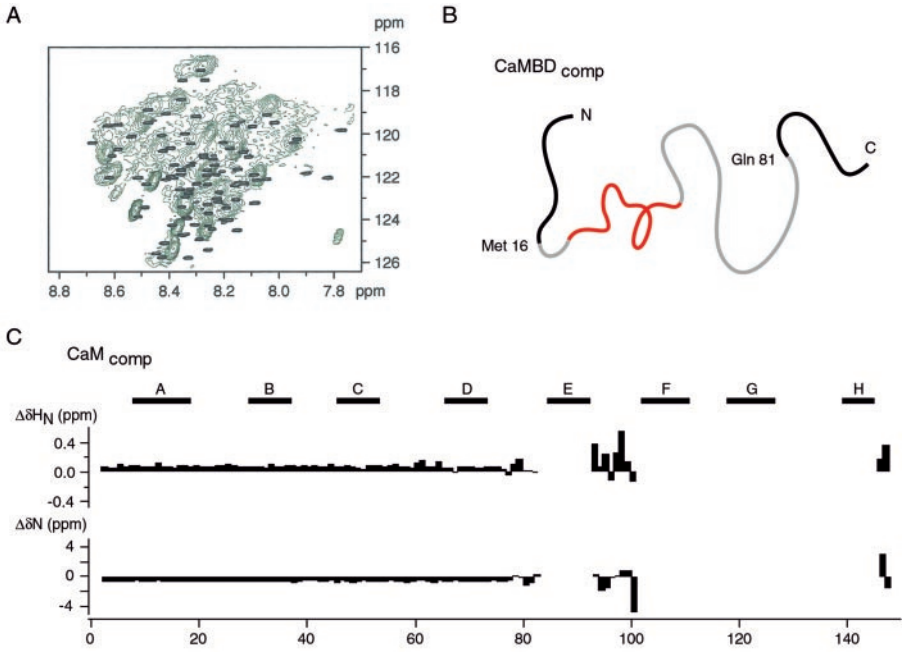

FIG. 6. **NMR data of the apo(CaMBD·CaM) complex.** *A*, part of a ^{1}H-^{15}N HSQC spectrum of CaMBD in uncomplexed (*black*) and complexed (*green*) form recorded at 600 MHz (298 K, 250 mM NaCl solution). *B*, cartoon illustrating CaMBD residues (*black*) exhibiting backbone amide cross-peaks in HSQC spectra. Note that only 16 amino acids at the N terminus and 11 residues at the C terminus of the molecule are visible; the remaining cross-peaks were broadened beyond the detection level. Residues 28–42 (corresponding to residues 423–437 in SK2) are drawn in *red*. *C*, differences in chemical shift observed for backbone HN groups between apoCaM in the complexed and uncomplexed form as a function of residue number; *black bars* designate the eight α-helices of apoCaM. Shift differences were calculated as δ (uncomplexed) minus δ (complexed) with shift values taken from a HSQC spectrum (uncomplexed) and a TROSY spectrum (complexed). Note that no significant chemical shift differences were observed for the N-terminal half of CaM, while for complexed CaM most residues in the C-terminal lobe could not be assigned with three-dimensional triple resonance experiments.

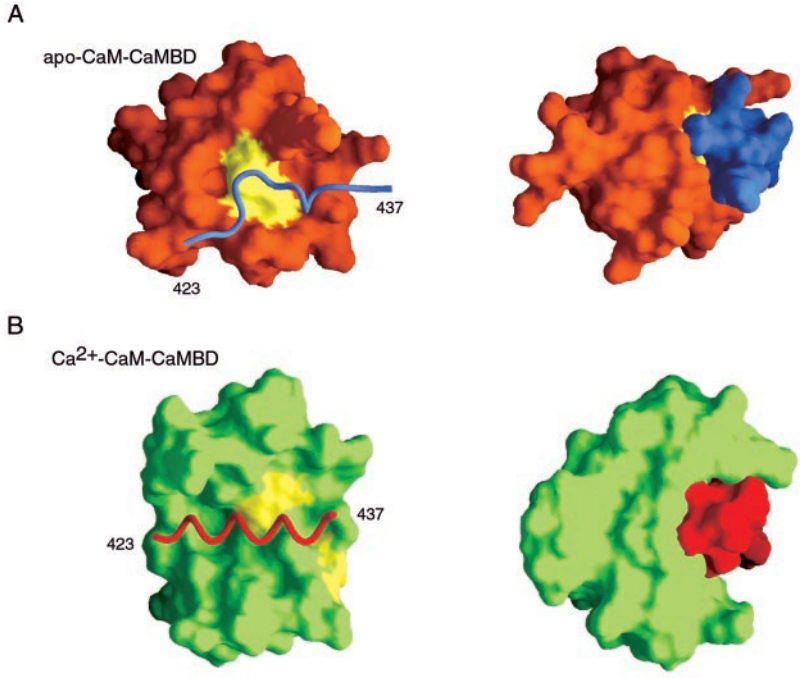

FIG. 7. **Assembly of CaMBD and apoCaM.** *A*, complex formation between the structured core region of CaMBD (residues 423–437) and the C-terminal lobe of apoCaM (37) as calculated by GRAMM (Ref. 24; see "Materials and Methods"). Left panel: CaMBD core (ribbon representation of the backbone) docked onto the C-terminal lobe of apoCaM (surface representation); right panel: both molecules in surface representation, rotated by 90° with respect to the left panel view. CaM-residues Met-124 and -144 are highlighted in *yellow*. *B*, complex between the core region of CaMBD and the C-terminal lobe of CaM as obtained upon cocrystallization of both molecules in the presence of 10 mM Ca^{2+} (Ref.17, PDB code 1G4Y). Both views are related as in *A*. Note the structural rearrangements in CaMBD as well as in the C-terminal lobe of CaM.

In summary, these data strongly suggest that complexation occurs between the C-terminal globular domain of apoCaM and the core region of CaMBD. In the complex, CaMBD seems to be in equilibrium between different conformational states rather than to present with a well defined structure.

DISCUSSION

Our results show that the solution structure of the SK2 CaMBD consists of highly flexible N and C termini that flank a well ordered core region forming an unusually folded helical domain between Ala-423 (Ala-28 in CaMBD) and Asn-437 (Asn-42 in CaMBD). Disruption of this domain in the isolated CaMBD or on the whole channel protein ablated Ca^{2+}-independent association of both molecules and thus abolished the Ca^{2+}-gating characteristic for SK type K^{+} channels (5, 10, 12).

The Ca^{2+}-independent association between CaM and CaMBD is an essential prerequisite for the rapid response to Ca^{2+} inherent in the physiological function of SK channels (11,

12). It seems likely that the interaction between CaM and the CaMBD of the channel subunits initially occurs during protein processing while the SK subunit is integrated into the endoplasmic reticulum membrane, exposing the CaMBD to the virtually Ca^{2+}-free cytoplasmic milieu.

Ca^{2+}-free interactions between the CaMBD and CaM occur in the C-terminal domain of CaM as concluded from functional analysis (11) as well as from NMR experiments on the apo(CaMBD·CaM) complex reconstituted in solution. The latter showed that complex formation involves stretches Met-17-Asp-80 of CaMBD and Glu-83-Lys-148 in the C-terminal globular domain of CaM. In the absence of Ca^{2+}, these sequence stretches undergo significant structural changes which, however, cannot be elucidated in detail due to conformational exchange processes on the intermediate time scale in the CaMBD core region.

Therefore, to get a more vivid picture of the complex formation, the associative process was simulated by "docking" the helical region of CaMBD (amino acids 423–437) onto the C-terminal globular domain of apoCaM as determined by NMR spectroscopy in solution (36). Fig. 7*A* illustrates the result with the best score (see "Materials and Methods"), showing that residues 423–437 of SK2 CaMBD fit snugly into a cleft of apoCaM where two methionines, Met-124 and Met-144, offer a hydrophobic pocket implicated previously to serve as a contact surface for interaction with target peptides (36). This finding is consistent with the result from the crystal of the Ca^{2+}-loaded CaMBD·CaM complex (17). This complex presents as a dimer composed of two CaM and two CaMBD molecules. Different from other CaM-target structures, bound Ca^{2+} ions were only found in the N-terminal lobe of CaM while the C-terminal EF-hands were free of Ca^{2+}. Nevertheless, the C-terminal lobe exhibited considerable structural reorganization with respect to the solution structure of apoCaM. These structural rearrangements allow CaM to tightly wrap around the N-terminal half of CaMBD (17). The intermolecular interface is formed by three "pockets" involving CaM residues Met-124 and Met-144 and by CaMBD residues 423–437 (Fig. 7*B*). In particular Ala-425 (Ala-30 in CaMBD), Leu-428 (Leu-33 in CaMBD) and Trp-432 (Trp-37 in CaMBD) were shown to tightly contact multiple hydrophobic surface patches on CaM.

As illustrated in Fig. 7*B*, the crystal structure shows that both CaM and the CaMBD undergo structural rearrangements in the complex. In CaM the secondary structural elements (helices αE, αF, αG, αH) forming the C-terminal lobe are largely repacked. In the CaMBD the core domain changed from the distorted helical folding observed in solution into a regular α-helical conformation. In this context, the conformational exchange seen in NMR experiments on the apo(CaMBD·CaM) complex may well result from an equilibrium between the distorted and regular folding of an α-helix.

While disrupting the helical domain in CaMBD and ablating Ca^{2+}-free interactions with CaM, the mutations at positions 427 and 428 did not interfere with interactions between the CaMBD and Ca^{2+}-loaded CaM (Fig. 5*A*), consistent with other structural and functional data (11, 17). This suggests that Ca^{2+}-dependent interactions are mediated by other regions of the CaMBD.

Therefore, the helical domain identified here by NMR may serve as a scaffold structure that binds Ca^{2+}-free CaM and participates in tethering it constitutively to the channel α-subunit. Upon calcification of the N-terminal EF-hands of CaM in the monomeric apo(CaMBD·CaM) complex (17), the Ca^{2+}-loaded CaMBD·CaM complex of one channel subunit dimerizes with the corresponding complex of one neighboring subunit, a transition that results in opening of the channel pore (17).

Coordinates—Atomic coordinates of the 23 best structures and the chemical shifts of SK2 CaMBD have been deposited in the Protein Data Bank (accession code 1KKD) and the BioMagResBank (accession code 5102), respectively.

Acknowledgments—We are grateful to H. R. Kalbitzer for spectrometer support, stimulating discussion, and reading of the manuscript. We thank Otogene AG (Tübingen, Germany) and the European Union-Large Scale Facility Florence (HPRI-CT-1999–00009) for access to their NMR spectrometers and D. Willbold for introducing us to GRAMM.

REFERENCES

1. Nicoll, R. A. (1988) *Science* **241,** 545–551
2. Pedarzani, P., Mosbacher, J., Rivard, A., Cingolani, L. A., Oliver, D., Stocker, M., Adelman, J. P., and Fakler, B. (2000) *J. Biol. Chem.* **276,** 9762–9769
3. Sah, P. (1996) *Trends Neurosci.* **4,** 150–154
4. Stocker, M., Krause, M., and Pedarzani, P. (1999) *Proc. Natl. Acad. Sci.* **96,** 4662–4667
5. Lancaster, B., and Adams, P. R. (1986) *J. Neurophys.* **55,** 1268–1282
6. Storm, J. F. (1990) *Prog. Brain Res.* **83,** 161–187
7. Kohler, M., Hirschberg, B., Bond, C. T., Kinzie, J. M., Marrion, N. V., Maylie, J., and Adelman, J. P. (1996) *Science* **273,** 1709–1714
8. Ishii, T. M., Silvia, C., Hirschberg, B., Bond, C. T., Adelman, J. P., and Maylie, J. (1997) *Proc. Natl. Acad. Sci. U. S. A.* **94,** 11651–11656
9. Joiner, W. J., Wang, L.-Y., Tang, M. D., and Kaczmarek, L. K. (1997) *Proc. Natl. Acad. Sci (U. S. A.)* **94,** 11013–11018
10. Fanger, C. M., Ghanshani, S., Logsdon, N. J., Rauer, H., Kalman, K., Zhou, J., Beckingham, K., Chandy, K. G., Cahalan, M. D., and Aiyar, J. (1999) *J. Biol. Chem.* **274,** 5746–5754
11. Keen, J. E., Khawaled, R., Farrens, D. L., Neelands, T., Rivard, A., Bond, C. T., Janowsky, A., Fakler, B., Adelman, J. P., and Maylie, J. (1999) *J. Neurosci.* **19,** 8830–8838
12. Xia, X. M., Fakler, B., Rivard, A., Wayman, G., Johnson-Pais, T., Keen, J. E., Ishii, T., Hirschberg, B., Bond, C. T., Lutsenko, S., Maylie, J., and Adelman, J. P. (1998) *Nature* **395,** 503–507
13. Ikura, M., Clore, G. M., Gronenborn, A. M., Zhu, G., Klee, C. B., and Bax, A. (1992) *Science* **256,** 632–638
14. Osawa, M., Tokumitsu, H., Swindells, M. B., Kurihara, H., Orita, M., Shibanuma, T., Furuya, T., and Ikura, M. (1999) *Nat. Struct. Biol.* **6,** 819–824
15. Rhoads, A. R., and Friedberg, F. (1997) *FASEB J.* **11,** 331–340
16. Swindells, M. B., and Ikura, M. (1996) *Nat. Struct. Biol.* **3,** 501–504
17. Schumacher, M., Rivard, A., Bächinger, H., and Adelman, J. P. (2001) *Nature* **410,** 1120–1124
18. Bartels, C., Xia, T. H., Billeter, M., Güntert, P., and Wüthrich, K. (1995) *J. Biomol. NMR* **5,** 1–10
19. Güntert, P., Mumenthaler, C., and Wuthrich, K. (1997) *J. Mol. Biol.* **273,** 283–298
20. Güntert, P., Braun, W., and Wuthrich, K. (1991) *J. Mol. Biol.* **217,** 517–530
21. Wüthrich, K. (1986) *NMR of Proteins and Nucleic Acids*, John Wiley & Sons, Inc., New York
22. Koradi, R., Billeter, M., and Wuthrich, K. (1996) *J. Mol. Graph.* **14,** 51–55
23. Nicholls, A., Sharp, K. A., and Honig, B. (1991) *Proteins* **11,** 281–296
24. Katchalski-Katzir, E., Shariv, I., Eisenstein, M., Friesem, A. A., Aflalo, C., and Vakser, I. A. (1992) *Proc. Natl. Acad. Sci. U. S. A.* **89,** 2195–2199
25. Vakser, I. A., and Aflalo, C. (1994) *Proteins* **20,** 320–329
26. Fakler, B., Brandle, U., Glowatzki, E., Weidemann, S., Zenner, H. P., and Ruppersberg, J. P. (1995) *Cell* **80,** 149–154
27. Fabiato, A. (1988) *Methods Enzymol.* **157,** 378–417
28. Antz, C., Bauer, T., Kalbacher, H., Frank, R., Covarrubias, M., Kalbitzer, H. R., Ruppersberg, J. P., Baukrowitz, T., and Fakler, B. (1999) *Nat. Struct. Biol.* **6,** 146–150
29. Klöcker, N., Oliver, D., Ruppersberg, J. P., Knaus, H. G., and Fakler, B. (2001) *Mol. Cell. Neurosci.* **17,** 514–520
30. Oliver, D., Klocker, N., Schuck, J., Baukrowitz, T., Ruppersberg, J. P., and Fakler, B. (2000) *Neuron* **26,** 595–601
31. Ishima, R., and Nagayama, K. (1995) *Biochemistry* **34,** 3162–3171
32. Brunger, A. T., Adams, P. D., Clore, G. M., DeLano, W. L., Gros, P., Grosse-Kunstleve, R. W., Jiang, J. S., Kuszewski, J., Nilges, M., Pannu, N. S., Read, R. J., Rice, L. M., Simonson, T., and Warren, G. L. (1998) *Acta Crystallogr. Sect. D Biol. Crystallogr.* **54,** 905–921
33. Wishart, D. S., and Sykes, B. D. (1994) *J. Biomol. NMR* **4,** 171–180
34. Chakrabartty, A., and Baldwin, R. L. (1995) *Adv. Protein Chem.* **46,** 141–176
35. Pervushin, K., Riek, R., Wider, G., and Wüthrich, K. (1997) *Proc. Natl. Acad. Sci. U. S. A.* **94,** 12366–12371
36. Zhang, M., Tanaka, T., and Ikura, M. (1995) *Nat. Struct. Biol.* **2,** 758–767
37. Geiser, J. R., van Tuinen, D., Brockerhoff, S. E., Neff, M. M., and Davis, T. N. (1991) *Cell* **65,** 949–959